

Ferromagnetism and possible heavy fermion behavior in single crystals of $\text{NdOs}_4\text{Sb}_{12}$

P.-C. Ho, W. M. Yuhasz, N. P. Butch, N. A. Frederick, T. A. Sayles, J. R. Jeffries, and M. B. Maple

*Department of Physics and Institute for Pure and Applied Physical Sciences,
University of California, San Diego, La Jolla, CA 92093-0360, U.S.A.*

J. B. Betts and A. H. Lacerda

National High Magnetic Field Laboratory/LANL, Los Alamos, NM 87545

P. Rogl

Institut fuer Physikalische Chemie, Universitaet Wien, A-1090 Wien, Wahringerstr. 42, Austria

G. Giester

Institut fuer Mineralogie und Kristallographie, Universitaet Wien, A-1090 Wien, Althanstr. 14, Austria

(Dated: July 02, 2005)

Single crystals of the filled-skutterudite compound $\text{NdOs}_4\text{Sb}_{12}$ have been investigated by means of electrical resistivity, magnetization, and specific heat measurements. The $\text{NdOs}_4\text{Sb}_{12}$ crystals have the $\text{LaFe}_4\text{P}_{12}$ -type cubic structure with a lattice parameter of 9.3 \AA . Possible heavy-fermion behavior is inferred from specific heat measurements, which reveal a large electronic specific heat coefficient $\gamma \approx 520 \text{ mJ/mol-K}^2$, corresponding to an effective mass $m^* \approx 98 m_e$. Features related to a ferromagnetic transition at $\sim 0.9 \text{ K}$ can be observed in electrical resistivity, magnetization and specific heat. Conventional Arrott-plot analysis indicates that $\text{NdOs}_4\text{Sb}_{12}$ conforms to mean-field ferromagnetism.

PACS numbers: 75.40.Cx, 71.27.+a, 71.70.Jp, 71.70.Ch

I. INTRODUCTION

The filled skutterudite compounds have the chemical formula MT_4X_{12} , where M is an alkali (Na or K), alkaline earth (Ca, Sr, Ba), lanthanide or actinide atom; T is a transition-metal atom (Fe, Ru, Os); and X is a pnictogen atom (P, As, Sb). The compounds crystallize in a $\text{LaFe}_4\text{P}_{12}$ -type structure with the space group $\text{Im}\bar{3}$.¹ Due to the strong hybridization between f- and conduction electrons and their unique crystal structure, the lanthanide- and actinide-based filled skutterudite materials display a wide range of strongly-correlated-electron phenomena, such as BCS-like superconductivity (e.g., $\text{PrRu}_4\text{Sb}_{12}$),^{2,3} heavy fermion behavior (e.g., $\text{PrFe}_4\text{P}_{12}$),⁴ heavy fermion superconductivity (e.g., $\text{PrOs}_4\text{Sb}_{12}$),^{5,6} ferromagnetism (e.g., $\text{PrFe}_4\text{Sb}_{12}$),⁷ metal-insulator transitions (e.g., $\text{PrRu}_4\text{P}_{12}$),⁸ Kondo-insulator behavior (e.g., $\text{UFe}_4\text{P}_{12}$ and $\text{CeFe}_4\text{P}_{12}$),⁹ valence fluctuation behavior (e.g., $\text{YbFe}_4\text{Sb}_{12}$),^{10,11} and non-Fermi-liquid behavior (e.g., $\text{CeRu}_4\text{Sb}_{12}$).^{12,13}

Previous studies have shown ferromagnetic ordering in Nd-based filled skutterudites. Measurements of $\text{NdFe}_4\text{Sb}_{12}$ revealed ferromagnetic order below 16.5 K with a Nd ordered moment of $2.04 \mu_B$ and a Fe collinear moment of $0.27 \mu_B$.¹⁴ Lower ferromagnetic transition temperatures were found in $\text{NdFe}_4\text{P}_{12}$ at 2 K ,¹⁵ $\text{NdRu}_4\text{P}_{12}$ at 1.6 K ,¹⁶ $\text{NdRu}_4\text{Sb}_{12}$ at 1.3 K ,^{2,3} and $\text{NdOs}_4\text{Sb}_{12}$ at 0.8 K .¹⁶ Since $\text{NdOs}_4\text{Sb}_{12}$ displays ferromagnetism with a low Curie temperature and its neighboring compound $\text{PrOs}_4\text{Sb}_{12}$ shows heavy fermion behavior and unconventional superconductivity,^{6,17,18,19,20} possibly involving triplet spin pairing of electrons, there

is a strong likelihood that $\text{PrOs}_4\text{Sb}_{12}$ is near a ferromagnetic quantum critical point. Thus, by thoroughly characterizing the physical properties of $\text{NdOs}_4\text{Sb}_{12}$, a deeper insight into the unusual behavior of $\text{PrOs}_4\text{Sb}_{12}$ may be attained. Earlier studies of the compound $\text{NdOs}_4\text{Sb}_{12}$ only reported the results of structural refinement²¹ and the value of the Curie temperature.¹⁶ In this report, we present a new and detailed investigation of $\text{NdOs}_4\text{Sb}_{12}$ single crystals, including measurements of X-ray diffraction, electrical resistivity, magnetization, and specific heat. We also discuss possible heavy fermion behavior in this Nd-based filled skutterudite compound.

II. EXPERIMENTAL DETAILS

$\text{NdOs}_4\text{Sb}_{12}$ single crystals were grown in a molten Sb flux as described previously,¹⁷ using high purity Nd, Os (3.5N), and Sb (6N). X-ray powder diffraction measurements were performed with a Rigaku D/MAX B x-ray machine on a powder prepared by grinding several single crystals, which indicated single phase $\text{NdOs}_4\text{Sb}_{12}$ with a minor impurity peak of Sb ($\lesssim 10\%$). The crystals had a $\text{LaFe}_4\text{P}_{12}$ -type BCC structure,¹ with a lattice parameter $a = 9.30 \text{ \AA}$. Two single crystals of similar dimension were selected for single crystal X-ray diffraction measurements. The data were collected on a four-circle Nonius Kappa diffractometer at 296 K using Mo K_α radiation ($\lambda = 0.071073 \text{ nm}$). No absorption corrections were necessary because of the rather regular crystal shape and small dimensions of the investigated crystals. The structure was refined with the SHELXS-97 program.²²

Electrical resistivity $\rho(T, H)$ was measured using the standard 4-wire technique in a Quantum Design PPMS system and in a ^3He - ^4He dilution refrigerator in fields up to 8 T. The low temperature (0.02 K - 2.6 K) and high-field (8 T - 18 T) $\rho(T, H)$ measurements were performed in the National High Magnetic Field Laboratory at Los Alamos National Laboratory. The electrical current applied to the sample was perpendicular to the applied magnetic field, which was along the [001] direction, in all $\rho(T, H)$ measurements. Measurements of $\rho(T, P)$ were made under hydrostatic pressures up to 28 kbar in a beryllium-copper piston-cylinder clamp²³ and a ^4He cryostat. The pressure was determined inductively from the pressure-dependent superconducting transition of a Pb manometer.

DC magnetic susceptibility from 2 K to 300 K was measured in a Quantum Design MPMS SQUID magnetometer. The magnetization $M(H, T)$ measurements were carried out in a ^3He Faraday magnetometer with a gradient field of ~ 0.05 - 0.1 T/cm in external fields up to 5.5 T and at temperatures between 0.4 K and 2 K. For the Faraday magnetometer measurements, several single crystals (total mass of 21.3 mg) were combined in a mosaic fashion and measurements were performed with magnetic field applied along the [001] axis. Specific heat $C(T)$ of multiple single crystals (total mass of 42.15 mg) was measured between 0.5 K and 70 K in a ^3He calorimeter using a semi-adiabatic heat-pulse technique.

III. RESULTS AND DISCUSSION

A. Single crystal structural refinement

Structural refinement was performed on X-ray diffraction data collected from single crystals of $\text{NdOs}_4\text{Sb}_{12}$; the results are listed in Table I. The thermal displacement parameters U_{ii} of the Nd atoms are isotropic and have large values compared with the U_{ii} for the Os and Sb atoms, a common feature in the filled skutterudites. The Nd sites are fully occupied, which is not always the case for filled skutterudites, such as $\text{Pr}_{0.73}\text{Fe}_4\text{Sb}_{12}$ and $\text{Eu}_{0.95}\text{Fe}_4\text{Sb}_{12}$.^{7,24} If the $\text{NdOs}_4\text{Sb}_{12}$ crystal is considered to be a simple Debye solid with the Nd atoms behaving like Einstein oscillators, the thermal displacement and the Einstein temperature Θ_E are related by

$$U = \frac{\hbar^2}{2m_{\text{Nd}}k_B\Theta_E} \coth\left(\frac{\Theta_E}{2T}\right), \quad (1)$$

where m_{Nd} is the atomic mass of Nd. For $\text{NdOs}_4\text{Sb}_{12}$, Θ_E is estimated as ~ 45 K, which is close to the values found for thallium-filled antimony skutterudites such as $\text{Tl}_{0.22}\text{Co}_4\text{Sb}_{12}$, $\text{Tl}_{0.5}\text{Co}_{3.5}\text{Fe}_{0.5}\text{Sb}_{12}$, $\text{Tl}_{0.8}\text{Co}_3\text{FeSb}_{12}$, and $\text{Tl}_{0.8}\text{Co}_4\text{Sb}_{11}\text{Sn}$.^{25,26}

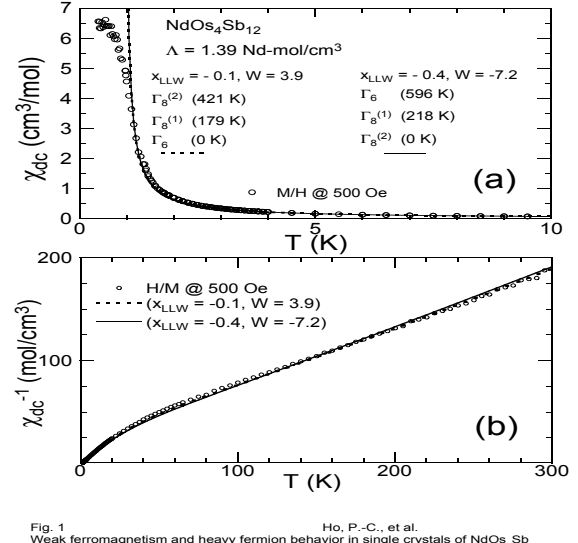


FIG. 1
Ho, P.-C., et al.
Weak ferromagnetism and heavy fermion behavior in single crystals of $\text{NdOs}_4\text{Sb}_{12}$

FIG. 1: (a) DC magnetic susceptibility χ_{dc} vs temperature T from 0 K to 10 K measured at 500 Oe. Fits of $\chi_{dc}(T)$ to a CEF model in which the ground state is either Γ_6 (dashed line) or $\Gamma_8^{(2)}$ (solid line). Below 10 K, these two lines overlap. (b) χ_{dc}^{-1} vs T from 0 K to 300 K. Fits of $\chi_{dc}(T)$ and $\chi_{dc}^{-1}(T)$ to a CEF model in which the ground state is either Γ_6 (dashed line) or $\Gamma_8^{(2)}$ (solid line).

B. Magnetic Properties

The dc magnetic susceptibility $\chi_{dc}(T)$ of $\text{NdOs}_4\text{Sb}_{12}$ was measured at 500 Oe and is displayed in Fig. 1(a). The $\chi_{dc}^{-1}(T)$ data (Fig. 1(b)) exhibit different slopes at high and low temperatures. The linear slope of $\chi_{dc}^{-1}(T)$ between 65 K and 300 K yields a Curie constant ($C_{\text{CW}} \equiv (N_A \mu_{\text{eff}}^2)/(3k_B)$) ~ 1.85 cm³K/mol, a negative Curie-Weiss temperature (Θ_{CW}) ~ -43 K, and an effective moment $\mu_{\text{eff}} \sim 3.84 \mu_B$, which is close to the Nd³⁺ free-ion value of $3.62 \mu_B$. The Curie-Weiss fit to the low-temperature range of $\chi_{dc}^{-1}(T)$ (Fig. 2(c)) gives $C_{\text{CW}} \sim 0.69$ cm³K/mol, a positive $\Theta_{\text{CW}} \sim 1$ K, and a value of $\mu_{\text{eff}} \sim 2.35 \mu_B$. The curvature in $\chi_{dc}^{-1}(T)$ is due to the influence of the crystalline electric field (CEF), and the positive Θ_{CW} from the low-temperature fit indicates ferromagnetic order developing below 1 K.

Although the crystal structure of $\text{NdOs}_4\text{Sb}_{12}$ has tetrahedral symmetry (T_h),²⁷ this is only a slight deviation from cubic symmetry (O_h). Thus, to simplify the CEF analysis, only O_h symmetry was considered. In an ionic (localized) model with cubic symmetry, the Nd³⁺ ten-fold degenerate $J = 9/2$ Hund's rule ground state multiplet splits into a Γ_6 doublet and two Γ_8 ($\Gamma_8^{(1)}, \Gamma_8^{(2)}$) quartet states. In the treatment of Lea, Leask, and Wolf,²⁸ these energy levels and their corresponding wave functions in cubic O_h symmetry can be parameterized by the variables x_{LLW} and W , where x_{LLW} is the ratio of the

TABLE I: Single crystal structural data measured at $T = 296$ K for $\text{NdOs}_4\text{Sb}_{12}$. The crystal structure is $\text{LaFe}_4\text{P}_{12}$ -type with the space group $\text{Im}\bar{3}$ (No. 204). The range of X-ray scattering angle is $2^\circ < 2\theta < 80^\circ$.

$\text{NdOs}_4\text{Sb}_{12}$			
Crystal size	$64 \times 78 \times 84 \mu\text{m}^3$	Lattice parameter a [Å]	9.3075(2)
Reflection in refinements	$473 \leq 4 \sigma(F_0)$ of 482	Number of variables	11
Goodness of fit	1.255		
Nd in 2a (0, 0, 0); Occupancy	1.00(1)	Thermal displacement $[\text{\AA}^2]$	
Os in 8c (1/4, 1/4, 1/4); Occupancy	1.00(1)	Thermal displacement $[\text{\AA}^2]$	
Sb in 24g (0, y, z); y: 0.15597(3) z: 0.34017(3) Occupancy	1.00(1)	Thermal displacement $[\text{\AA}^2]$	
		Sb: U_{11}	0.0026(1)
		U_{22}	0.0044(1)
		U_{33}	0.0065(1)
		Interatomic distances [Å]	
		Nd - 12 Sb	3.4831
		Interatomic distances [Å]	
		Os - 6 Sb	2.6239
		Interatomic distances [Å]	
		Sb - 1 Sb	2.9033
		- 1 Sb	2.9752
		- 2 Os	2.6239
		- 1 Nd	3.4831

fourth- and sixth-order terms of the angular momentum operators and W is an overall energy scale. The CEF contribution to the molar magnetic susceptibility can be determined from the expression²⁹

$$\chi_{\text{CEF}}(T) = N_A g_J^2 \mu_B^2 \left[\sum_i \frac{|\langle i | J_z | i \rangle|^2}{k_B T} p_i - 2 \sum_{i,j(\neq i)} \frac{|\langle i | J_z | j \rangle|^2}{E_i - E_j} p_i \right] \quad (2)$$

where N_A is Avogadro's number, g_J is the Landé g-factor, μ_B is the Bohr magneton, $p_i = e^{-E_i/(k_B T)}/Z$ is the thermal population probability (Z is the partition function), and the E_i 's are the energies of the multiplets. However, the occurrence of ferromagnetic order in $\text{NdOs}_4\text{Sb}_{12}$ requires the presence of a molecular field constant Λ to account for the effective field, with $\chi^{-1} = \chi_{\text{CEF}}^{-1} - \Lambda$.

The low-temperature value of μ_{eff} ($2.35 \mu_B$) indicates that the ground state of Nd^{3+} is either Γ_6 or $\Gamma_8^{(2)}$. A wide range of x_{LLW} values with a Γ_6 ground state can fit the $\chi(T)$ data reasonably well ($-1 \leq x_{\text{LLW}} \leq 0.1$). For a Γ_8 ground state, a good fit to the $\chi(T)$ data is only found for $x_{\text{LLW}} \approx -0.4$. All the fits imply that the splitting between the ground and first excited states is greater than 120 K. When compared with the $\rho(T)$ data (to be discussed later), the best fits are (I) $x_{\text{LLW}} = -0.1$, $W = 3.9$, and (II) $x_{\text{LLW}} = -0.4$, $W = -7.2$, corresponding to the following level schemes: (I) Γ_6 (0 K), $\Gamma_8^{(1)}$ (180 K), $\Gamma_8^{(2)}$ (420 K) and (II) $\Gamma_8^{(2)}$ (0 K), $\Gamma_8^{(1)}$ (220 K), Γ_6 (600 K), with $\Lambda = 1.39 \text{ Nd-mol/cm}^3$ and an effective ground state moment $\sim 2.31 \mu_B$ for both schemes. These fits are displayed in Figs. 1(a) and (b). The Heisenberg interaction strength between a Nd ion and its eight nearest neighbors is estimated to be 0.522 K from Λ .

Isothermal magnetization measurements $M(H)$, displayed in Fig. 2(a), were made above and below the Curie temperature (Θ_C). In the paramagnetic state, the $M(H)$ isotherms between 2 K and 5 K can be fit well by a Brillouin function with effective $J = 2.7$ that includes a temperature shift of 1 K due to ferromagnetism. The $M(H)$ isotherms in the vicinity of Θ_C were used to construct a conventional Arrott plot consisting of M^2 vs H/M isotherms, shown in Fig. 2(b). The isotherms in the Arrott plot are linear and parallel in the vicinity of Θ_C for $H \leq 1$ T, indicating that $\text{NdOs}_4\text{Sb}_{12}$ is a mean-field fer-

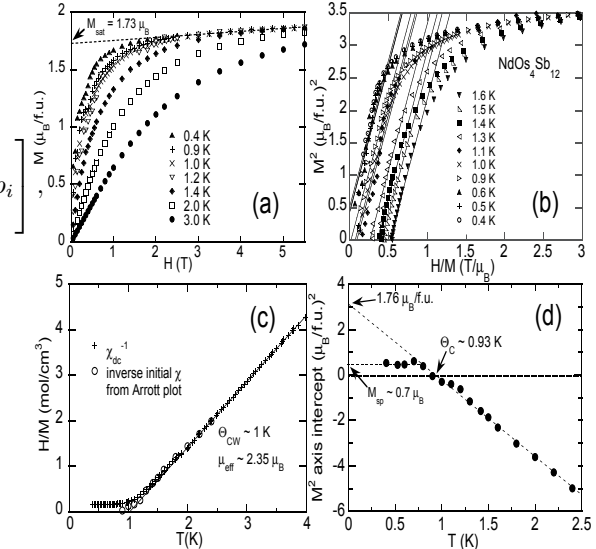


Fig. 2: (a) Magnetization M vs magnetic field H isotherms and the saturation magnetization M_{sat} determined from M vs H isotherms below the Curie temperature Θ_C . (b) M^2 vs H/M isotherms (Arrott plot) for $\text{NdOs}_4\text{Sb}_{12}$. (c) Inverse initial magnetic susceptibility (open circles) determined from $M^2 = 0$ intercepts of M^2 vs H/M isotherms, compared to the $\chi_{\text{dc}}^{-1}(T)$ data (pluses). The line is a Curie-Weiss fit. (d) $H/M = 0$ intercepts of M^2 vs H/M isotherms plotted versus T . Positive values correspond to the spontaneous magnetization M_{sp} .

FIG. 2: (a) Magnetization M vs magnetic field H isotherms and the saturation magnetization M_{sat} determined from M vs H isotherms below the Curie temperature Θ_C . (b) M^2 vs H/M isotherms (Arrott plot) for $\text{NdOs}_4\text{Sb}_{12}$. (c) Inverse initial magnetic susceptibility (open circles) determined from $M^2 = 0$ intercepts of M^2 vs H/M isotherms, compared to the $\chi_{\text{dc}}^{-1}(T)$ data (pluses). The line is a Curie-Weiss fit. (d) $H/M = 0$ intercepts of M^2 vs H/M isotherms plotted versus T . Positive values correspond to the spontaneous magnetization M_{sp} .

romagnet. The intercepts of the linear fits to the (H/M) axis (\equiv the inverse initial magnetic susceptibility) agree well with the low-temperature $\chi_{\text{dc}}^{-1}(T)$ data (Fig. 2(c)). The intercepts of the linear fit to the M^2 axis are shown in Fig. 2(d), where zero identifies $\Theta_C = 0.93$ K. Below Θ_C , the intercept of the M^2 -axis corresponds to the square of the spontaneous magnetization (M_{sp}^2), which levels off and results in a small value of $M_{\text{sp}} \sim 0.7 \mu_B$. However, a linear extrapolation of the negative M^2 -axis intercept back to zero temperature yields a much larger value of $\sim 1.76 \mu_B/\text{f.u.}$, which is comparable to the saturation magnetization M_{sat} of $\sim 1.73 \mu_B/\text{f.u.}$ determined

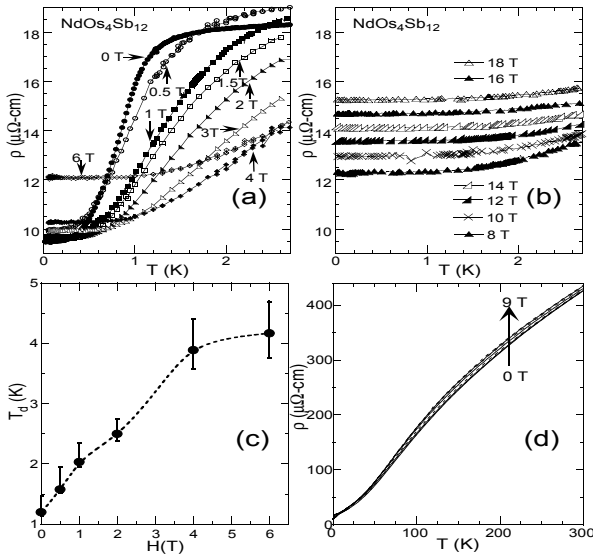


Fig. 3 Ho, P.-C., et al.: Weak ferromagnetism and heavy fermion behavior in single crystals of $\text{NdOs}_4\text{Sb}_{12}$

FIG. 3: (a) Low-temperature electrical resistivity ρ vs temperature T for magnetic fields H between 0 T and 6 T for $\text{NdOs}_4\text{Sb}_{12}$. The solid lines are guides to the eye. (b) Low-temperature electrical resistivity ρ vs T for magnetic fields H between 8 T and 18 T for $\text{NdOs}_4\text{Sb}_{12}$. The solid lines are guides to the eye. (c) Position of the shoulder T_d in $\rho(T)$ (which corresponds to Θ_C) vs H , with vertical bars indicating the width of the transition at T_d as described in the text. (d) High- T resistivity ρ vs T at $H = 0$ T, 0.5 T, 1 T, 2 T, 4 T, 6 T, 8 T, 9 T.

directly from the $M(H)$ data of $\text{NdOs}_4\text{Sb}_{12}$ (Fig. 2(a)). The value of M_{sat} is also consistent with the saturation magnetization found in $\text{NdFe}_4\text{P}_{12}$ ($1.72 \mu_B/\text{f.u.}$).¹⁵

C. Electrical Resistivity

Low-temperature electrical resistivity $\rho(T)$ data for $\text{NdOs}_4\text{Sb}_{12}$ in various magnetic fields from 0 T to 18 T are shown in Figs. 3(a) and (b). The zero-field residual resistivity ratio $\text{RRR} \equiv \rho(300\text{ K})/\rho(0.02\text{ K})$ of ~ 45 indicates that the single crystal studied is of good metallurgical quality (Fig. 3(a) and (d)). A shoulder occurs in the zero-field $\rho(T)$ curve at ~ 1.2 K, below which $\rho(T)$ has a sharp drop, indicating the development of an ordered state. The temperature T_d at which this drop occurs is defined as the intercept of two lines, one of which is a linear fit to the data above the transition while the other is a linear fit to the data below the transition. The upper and lower limits of the transition are defined as the temperatures midway between T_d and the temperatures at which the data deviate from the linear fits. Shown in Fig. 3(c) is the field dependence of T_d , which increases with increasing field up to 6 T, and is no longer observed in the $\rho(T)$ data at higher fields. The temperature T_d correlates with the onset of ferromagnetic order at 0.9 K determined from magnetization and specific heat measure-

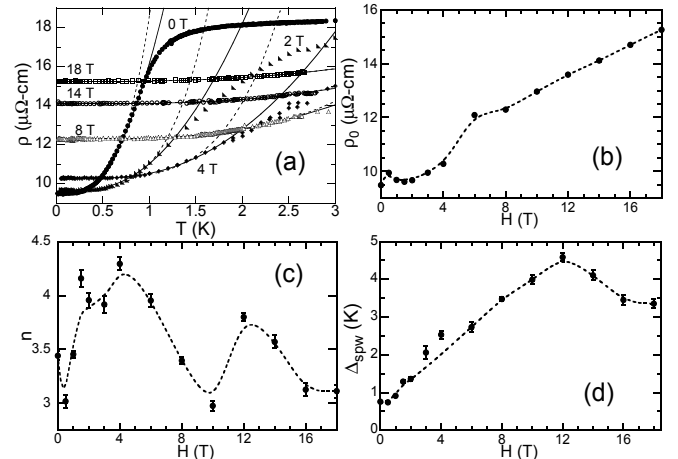


Fig. 4 Ho, P.-C., et al.: Weak ferromagnetism and heavy fermion behavior in single crystals of $\text{NdOs}_4\text{Sb}_{12}$

FIG. 4: (a) Low- T electrical resistivity ρ vs temperature T with power-law (dashed line) and spin-wave (solid line) fits at various magnetic fields for $\text{NdOs}_4\text{Sb}_{12}$. (b) Residual resistivity ρ_0 vs H . (c) Exponent n of the power-law fit vs H . (d) Energy gap Δ_{spw} from the spin-wave fit vs H .

ments. Displayed in Fig. 3(d) are the high-temperature $\rho(T, 0 \text{ T} \leq H \leq 9 \text{ T})$ data for $\text{NdOs}_4\text{Sb}_{12}$, which show a slight increase in $\rho(T)$ with increasing field.

In order to analyze the behavior of the resistivity below Θ_C , the $\rho(T)$ data were fit with a power-law of the form $\rho(T) = \rho_0 + BT^n$. The fitting curves are plotted as dashed lines in Fig. 4(a). The residual resistivity ρ_0 increases with increasing field and has a linear H -dependence above 8 T (Fig. 4(b)). Between 0 T and 18 T, the exponent n varies from 3 to 4, which indicates that $\text{NdOs}_4\text{Sb}_{12}$ exhibits neither typical Fermi-liquid ($n \sim 2$) nor typical non-Fermi-liquid ($n < 2$) behavior (Fig. 4(c)). Since ferromagnetic ordering occurs below Θ_C , electron-spin wave scattering was considered with the form³⁰

$$\rho(T) = \rho_0 + A \frac{T}{\Delta_{\text{spw}}} \left(1 + 2 \frac{T}{\Delta_{\text{spw}}} \right) \exp \left(-\frac{\Delta_{\text{spw}}}{T} \right), \quad (3)$$

where Δ_{spw} is the spin wave energy gap, which may result either from magnetic anisotropy or from broken symmetry due to presence of a CEF. This formula describes the $\rho(T, H)$ data well, and the fitting curves are shown as solid lines in Fig. 4(a). As determined from these fits, the spin-wave energy gap Δ_{spw} is ~ 0.75 K at 0 T, increases approximately linearly to ~ 4.5 K as the field increases to 12 T, and then drops to ~ 3.4 K at 18 T (Fig. 4(d)).

Figure 5(a) displays the zero-field $\rho(T)$ data, which have a slight negative curvature at ~ 130 K that may be related to scattering from the CEF levels. In order to analyze the CEF contribution to $\rho(T)$ at 0 T, it is necessary to subtract a lattice contribution $\rho_{\text{lat}}(T)$ and an impurity contribution ρ_{imp} ($\sim 9.4 \mu\Omega\text{-cm}$) from the resistivity data. Usually, $\rho_{\text{lat}}(T)$ is estimated from an isostructural nonmagnetic reference compound; in the

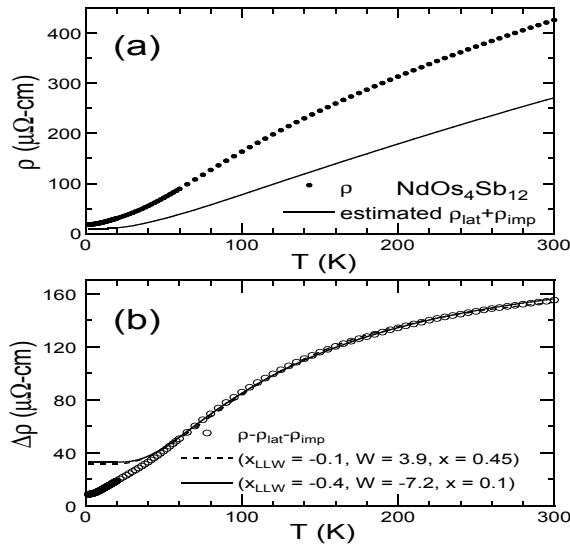


Fig. 5
Ho, P.-C., et al.
Weak ferromagnetism and heavy fermion behavior in single crystals of $\text{NdOs}_4\text{Sb}_{12}$

FIG. 5: (a) Zero-field resistivity ρ and the estimated $\rho_{\text{lat}} + \rho_{\text{imp}}$ vs temperature T for $\text{NdOs}_4\text{Sb}_{12}$, where $\rho_{\text{imp}} \sim 9.4 \mu\Omega\text{-cm}$. (b) Temperature dependence of the incremental resistivity $\Delta\rho = \rho - \rho_{\text{lat}} - \rho_{\text{imp}}$ and CEF fits for two different ground states: Γ_6 (dashed line) and $\Gamma_8^{(2)}$ (solid line), where $x/(1-x)$ is the ratio of s-f exchange to aspherical Coulomb scattering for $\text{NdOs}_4\text{Sb}_{12}$.

case of $\text{NdOs}_4\text{Sb}_{12}$, the resistivity of $\text{LaOs}_4\text{Sb}_{12}$, which has an empty 4-f shell, was used. However, above 100 K, $\rho(T)$ of $\text{LaOs}_4\text{Sb}_{12}$ exhibits a significant negative curvature that is common in La-based compounds such as LaAl_2 .^{31,32} This curvature is generally less pronounced in Sc-, Y-, and Lu-based compounds, which have completely empty or filled 4f-electron shells. However, the compounds $\text{ScOs}_4\text{Sb}_{12}$, $\text{YO}_4\text{Sb}_{12}$ and $\text{LuOs}_4\text{Sb}_{12}$ have not yet been synthesized. Above 100 K, $\rho_{\text{lat}}(T)$ was estimated from $\text{SmOs}_4\text{Sb}_{12}$, as $\rho(T)$ of $\text{SmOs}_4\text{Sb}_{12}$ has an approximately linear- T dependence between 100 K and 300 K.³³ The s-f exchange scattering effect in $\rho(T)$ of $\text{SmOs}_4\text{Sb}_{12}$ only appears below 80 K due to the small energy splitting (~ 35 K) between the ground and the first excited states in that compound. Thus it is reasonable to assume that $\rho(T)$ of $\text{SmOs}_4\text{Sb}_{12}$ for $100 \text{ K} \leq T \leq 300 \text{ K}$ is due to electron-phonon scattering and use it as an estimate of the high-temperature portion of $\rho_{\text{lat}}(T)$ for $\text{NdOs}_4\text{Sb}_{12}$.

The incremental resistivity $\Delta\rho(T) = \rho(T) - \rho_{\text{lat}}(T) - \rho_{\text{imp}}$ (Fig. 5(b)) is best described by two energy-level schemes that are consistent with the CEF analysis of $\chi(T)$ discussed previously. During the CEF analysis of $\Delta\rho(T)$, it was also found that s-f exchange scattering alone could not entirely account for $\Delta\rho(T)$; otherwise, ρ_{imp} would always be negative, which is unphysical. Thus, the effect of aspherical Coulomb scattering^{34,35,36} was also considered, with the ratio between the s-f exchange scattering and the aspherical Coulomb scattering

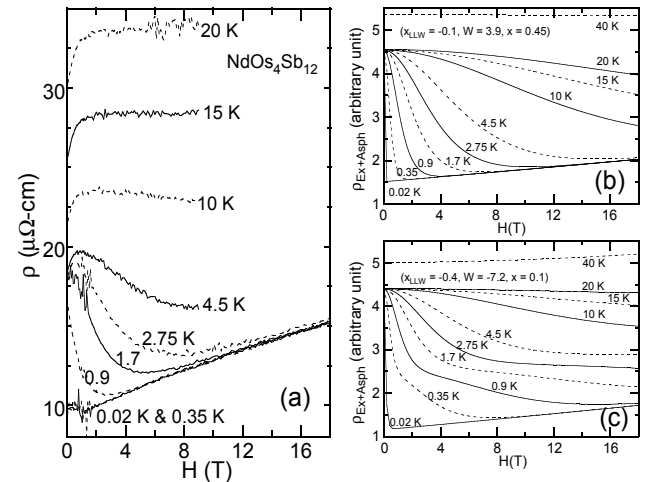


Fig. 6
Ho, P.-C., et al.
Weak ferromagnetism and heavy fermion behavior in single crystals of $\text{NdOs}_4\text{Sb}_{12}$

FIG. 6: (a) Isotherms of electrical resistivity ρ vs magnetic field H for $\text{NdOs}_4\text{Sb}_{12}$. (b) and (c) Calculated ρ vs H isotherms including the effects of s-f exchange and aspherical Coulomb scattering using the CEF parameters determined from zero-field data.

defined as $x : (1-x)$. In Fig. 5(b), the fit curves representing the two best-fit energy schemes are plotted in comparison with $\Delta\rho(T)$, which is described well by both fits above 40 K. The departure of $\Delta\rho(T)$ from the fits below 40 K may be due to a reduction of the electron scattering, resulting from the development of the coherent heavy-fermion ground state in $\text{NdOs}_4\text{Sb}_{12}$ as the temperature is lowered. The $\rho(H)$ isotherms are displayed in Fig. 6(a) and qualitatively agree with the $\rho(H)$ isotherms generated using the cubic-CEF parameters determined from the zero-field fits to $\Delta\rho(T)$ (Figs. 6(b) and (c)).

Measurements of $\rho(T)$ were performed from 1 K to 300 K under nearly hydrostatic pressure P between 0 kbar and 28 kbar (Fig. 7). In Fig. 7 it can clearly be seen that the pressure-induced change in the high- T electrical resistivity is much more pronounced than the resistivity change induced by high field (Fig. 3(c)), in the pressure and temperature ranges of this investigation. However, at low temperatures, the value of T_d is more strongly influenced by an increase in field H (Fig. 3(b)) than by variation of P (Fig. 7 inset (b)).

D. Specific Heat

Specific heat divided by temperature C/T vs T data for $\text{NdOs}_4\text{Sb}_{12}$ are shown in Fig. 8(a). The data reveal a pronounced peak at ~ 0.8 K that correlates well with the magnetic ordering temperature Θ_C inferred from the shoulder of $\rho(T)$, the divergence of $\chi_{\text{dc}}(T)$, and the Arrott-plot analysis. No obvious Schottky anomaly associated with CEF energy splitting was observed in the $C(T)$ data below 20 K. This is consistent with the fact

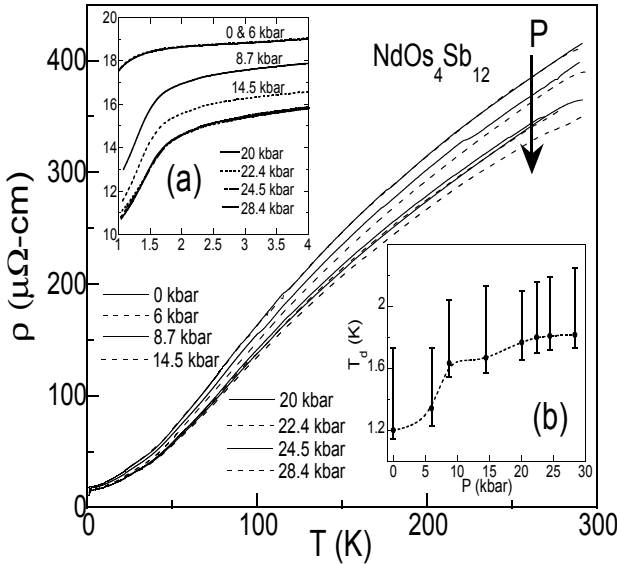


Fig. 7
Ho, P.-C., et al.
Weak ferromagnetism and heavy fermion behavior in single crystals of $\text{NdOs}_4\text{Sb}_{12}$

FIG. 7: Electrical resistivity ρ vs temperature T for $\text{NdOs}_4\text{Sb}_{12}$ at various pressures P up to 28 kbar. Inset (a): Expanded view of the resistive ferromagnetic transitions. Inset (b): Temperature of the drop in $\rho(T)$ due to the onset of ferromagnetism T_d (approximately corresponding to the Curie temperature Θ_C) vs P with vertical bars indicating the width of the transition.

that all the fits to the dc magnetic susceptibility data imply that the CEF splitting between the ground and first excited states is greater than 120 K. The Schottky anomaly due to 120 K CEF splitting would exhibit a peak at ~ 40 K and make a negligible contribution to $C(T)$ 20 K. Such a peak would also be difficult to resolve against the large lattice background.

In Fig. 8(a), the specific heat of $\text{LaOs}_4\text{Sb}_{12}$ is displayed in comparison with that of $\text{NdOs}_4\text{Sb}_{12}$, where the electronic specific heat coefficient γ and the Debye temperature Θ_D of $\text{LaOs}_4\text{Sb}_{12}$ are $\sim 36 \text{ mJ/mol-K}^2$ and ~ 280 K, respectively. After the specific heat of nonmagnetic $\text{LaOs}_4\text{Sb}_{12}$ (an estimate of the lattice heat capacity of $\text{NdOs}_4\text{Sb}_{12}$) is subtracted from the specific heat of $\text{NdOs}_4\text{Sb}_{12}$, the difference divided by temperature $\delta C/T$ is plotted against T^2 and shown in the inset of Fig. 8(a). The value of γ for $\text{NdOs}_4\text{Sb}_{12}$ estimated from the $\delta C/T$ vs T^2 plot ranges from $\sim 436 \text{ mJ/mol-K}^2$ to $\sim 530 \text{ mJ/mol-K}^2$. Below 13 K, $\delta C/T$ vs T^2 is not constant, which could be due to a difference between the actual lattice heat capacities of $\text{NdOs}_4\text{Sb}_{12}$ and $\text{LaOs}_4\text{Sb}_{12}$. Nevertheless, the curvature in C/T vs T^2 of $\text{NdOs}_4\text{Sb}_{12}$ (inset of Fig. 8(b)) and the magnetic transition occurring at ~ 1 K cause difficulties in the analysis of the data using the typical formula $C/T = \gamma + \beta T^2$. Since we have strong evidence against the possibility of a CEF Schottky contribution from the analysis of the $\chi(T)$ data, the curvature in C/T vs T^2 is possibly due to either the rat-

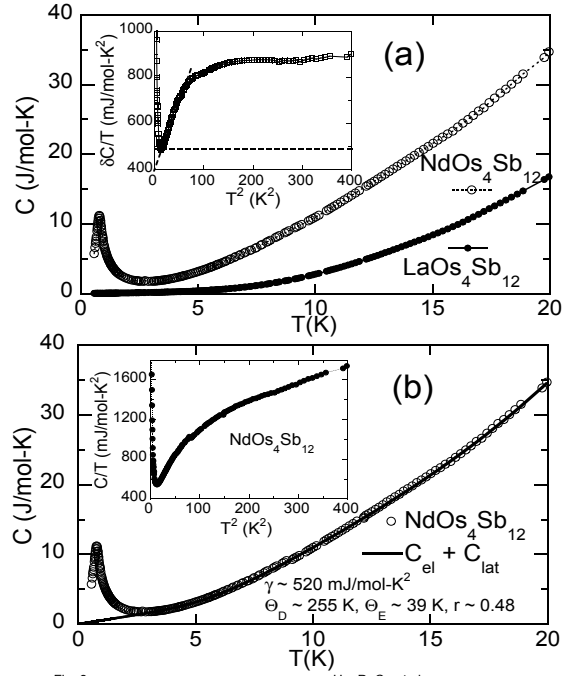


Fig. 8
Ho, P.-C., et al.
Weak ferromagnetism and heavy fermion behavior in single crystals of $\text{NdOs}_4\text{Sb}_{12}$

FIG. 8: (a) Zero-field C vs T for $\text{NdOs}_4\text{Sb}_{12}$ and $\text{LaOs}_4\text{Sb}_{12}$ below 20 K. Inset: $\delta C/T$ vs T^2 below 20 K, where $\delta C \equiv C(\text{NdOs}_4\text{Sb}_{12}) - C(\text{LaOs}_4\text{Sb}_{12})$. The extrapolated values of the two dashed lines at 0 K set the lower and upper limits of $\gamma(\text{NdOs}_4\text{Sb}_{12}) - \gamma(\text{LaOs}_4\text{Sb}_{12})$. (b) A comparison between C of $\text{NdOs}_4\text{Sb}_{12}$ and a fit of $C_{\text{el}} + C_{\text{lat}}$, where $C_{\text{el}} = \gamma T$ and C_{lat} is composed of C_{Deb} and C_{Ein} as described in the text. The electronic specific heat coefficient γ , the Debye temperature (Θ_D), the Einstein temperature (Θ_E), and the coupling constant r for the Einstein oscillator are estimated as 520 mJ/mol-K^2 , 255 K, 39 K and 0.48 respectively. Inset: C/T vs T^2 for $\text{NdOs}_4\text{Sb}_{12}$ below 20 K for $\text{NdOs}_4\text{Sb}_{12}$.

ting motion of the Nd atoms or a narrow peak in the density of electronic states near Fermi energy, such as a Kondo resonance.³⁷ However, we do not consider the application of the resonance level model (RLM)³⁷ to be appropriate, because the magnetization data above Θ_C are fit well by a Brillouin function and no obvious Kondo effect is observed in the $\rho(T)$ data of $\text{NdOs}_4\text{Sb}_{12}$. In the previous specific heat studies of the $\text{Ti}_{0.22}\text{Co}_4\text{Sb}_{12}$ filled skutterudite compound, Sales et al.²⁵ found that the difference in heat capacity between $\text{Ti}_{0.22}\text{Co}_4\text{Sb}_{12}$ and the unfilled skutterudite compound $\text{Co}_4\text{Sb}_{12}$ can be accurately described by a quantized oscillator (Einstein model) with an Einstein temperature Θ_E of 55 K. Since the X-ray structural refinement at room temperature for $\text{NdOs}_4\text{Sb}_{12}$ indicates a small $\Theta_E \sim 45$ K associated with the Nd atoms, it can be assumed that the Nd atoms partially act like Einstein oscillators with a mixing ratio r , and the lattice contribution to the specific heat can be

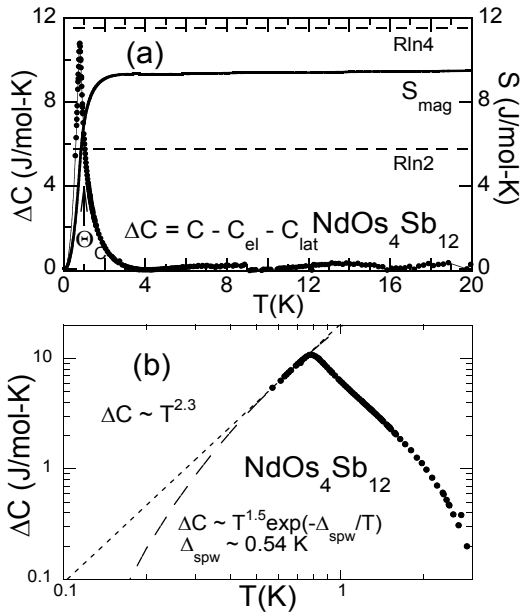


Fig. 9
Weak ferromagnetism and heavy fermion behavior in single crystals of NdOs₄Sb₁₂
Ho, P.-C., et al.

FIG. 9: (a) Incremental specific heat ΔC ($\Delta C \equiv C - C_{el} - C_{lat}$) (left axis) and the magnetic entropy S_{mag} (right axis) vs temperature T . (b) Logarithmic plot of the power-law fit (dotted line) and the anisotropic-spin-wave fit (dashed line) to the incremental specific heat $\Delta C(T)$ after the electronic and lattice contributions have been removed (in a very limited measuring range below Θ_C).

expressed as $C_{lat} = C_{Ein} + C_{Deb}$,

$$C_{Ein} = r \left[3R \frac{(\Theta_E/T)^2 e^{(\Theta_E/T)}}{[e^{(\Theta_E/T)} - 1]^2} \right], \quad (4)$$

$$C_{Deb} = (17 - r) \cdot \frac{12\pi^4}{5} R \left(\frac{T}{\Theta_D} \right)^3, \quad (5)$$

where R is the universal gas constant, Θ_D represents the Debye temperature, and $r \leq 1$. The effective Debye contribution is $(17 - r)/r$ times bigger than that of the Einstein-like Nd rattling motion due to the participation of the rest of the atoms in the unit cell. Below 20 K, a least squares fit of $C_{el} + C_{lat}$ to the $C(T)$ data was performed, where $C_{el} = \gamma T$ is the electronic specific heat, from which estimated values of γ , Θ_D , Θ_E , and r were derived. The fitting curve is plotted in Fig. 8(b) along with the $C(T)$ data of NdOs₄Sb₁₂ as a comparison. The values obtained for γ , Θ_D , Θ_E , and r are estimated as 520 mJ/mol-K², 255 K, 39 K, and 0.48, respectively. The value of Θ_D is close to the Debye temperature of LaOs₄Sb₁₂, the value of Θ_E is comparable to that determined from the X-ray data, and the value of γ is close to that estimated from the simple subtraction of the LaOs₄Sb₁₂ specific heat data, suggesting that NdOs₄Sb₁₂ is possibly a heavy fermion compound.

The temperature dependence of the magnetic entropy S_{mag} was derived from the integration of $\Delta C/T$ vs T and is shown in Fig. 9(a), where $\Delta C \equiv C - C_{el} - C_{lat}$. The magnetic entropy (S_{mag}) in NdOs₄Sb₁₂ reaches 0.69R (\approx Rln4) at 0.85 K and levels off at a value of $\sim 1.14R$ (\approx Rln3). The magnetic entropy reaches $\sim 74\%$ of its full value at Θ_C , and a noticeable magnetic contribution persists up to ~ 3 K, revealing the existence of magnetic fluctuations above Θ_C . It has been argued for the antiferromagnetic system Gd_{1-x}Y_xNi₂Si₂ that magnetic fluctuations can contribute to $C(T)$ at temperatures up to 5 times the Néel temperature.³⁸ Thus, we cannot completely rule out the possibility that the short range magnetic correlations near the ferromagnetic transition temperature regime give rise to enhancement of the specific heat of NdOs₄Sb₁₂.^{38,39,40} However, it is unlikely that they would account for a large fraction of the enhanced specific heat, due to the following arguments: (i) The paramagnetic-state $M(H)$ isotherm data (2 - 5 K) scale well with a Brillouin function. The $M(H)$ data at 2 K and 3 K, and the $\chi_{dc}^{-1}(T)$ data along with the initial χ^{-1} from the Arrott Plot analysis do not show obvious evidence of magnetic fluctuations above 2 K (displayed in Fig. 2 (a) and (b)). (ii) The value estimated for γ (520 mJ/mol-K²) is within the upper and lower limits of γ (436 - 530 mJ/mol-K²) estimated from the analysis done by comparing the specific heat of NdOs₄Sb₁₂ with that of the nonmagnetic compound LaOs₄Sb₁₂ suggesting that our analysis is justified. (iii) The lower limit (4 K) of the fitting range used to determine γ from the formula $C = C_{el} + C_{lat}$ is four times the Curie temperature, which is safely higher than the temperature at which the calculated S_{mag} saturates. (iv) Heavy fermion behavior has been found in the neighboring compounds PrOs₄Sb₁₂ ($\gamma \sim 600$ mJ/mol-K²)⁴¹ and SmOs₄Sb₁₂ ($\gamma \approx 880$ mJ/mol-K²);³³ earlier studies of the related compound NdFe₄Sb₁₂ also reported possible evidence for an enhanced electron mass.^{15,42} Considering all of these points, it seems likely that NdOs₄Sb₁₂ displays heavy fermion behavior.

Since S_{mag} lies between Rln2 ($= 0.69R$) and Rln4 ($= 1.39R$), it is difficult to determine conclusively whether the Γ_6 doublet or $\Gamma_8^{(2)}$ quartet is the Nd³⁺ ground state. If the Γ_6 doublet is the ground state, then the extra entropy may result from another degree of freedom, such as a tunnelling mode or off-center mode of Nd³⁺ ion in an Sb-icosahedron cage.⁴³ If the $\Gamma_8^{(2)}$ quartet is the ground state, the smaller entropy may be due to an overestimated lattice contribution to the specific heat or transfer of entropy to the conduction electron system.

Figure 9(b) displays the incremental specific heat $\Delta C(T)$ after the electronic and lattice contributions have been removed. Even though the range of the $\Delta C(T)$ data below Θ_C is very limited, the data were fit with spin-wave formulas $\Delta C(T) \propto T^n$ for magnetically isotropic metals and $\Delta C(T) \propto T^{3/2} \exp(-\Delta_{spw}/T)$ for magnetically anisotropic metals.⁴⁴ From the first formula, the value of the exponent $n \approx 2.3$ is higher than the value of

1.5 expected from a spin wave in an isotropic metal. The spin-wave energy gap Δ_{spw} determined from the second formula is ~ 0.54 K, consistent with the value of 0.75 K determined from the zero-field resistivity data.

IV. SUMMARY

We have performed X-ray diffraction, electrical resistivity, magnetization, and specific heat studies of $\text{NdOs}_4\text{Sb}_{12}$ single crystals, which exhibit interesting strongly-correlated-electron behavior. X-ray experiments have revealed full occupancy of Nd sites and a large mean square displacement of Nd ions in $\text{NdOs}_4\text{Sb}_{12}$. The compound $\text{NdOs}_4\text{Sb}_{12}$ exhibits mean-field-type ferromagnetism with $\Theta_C \sim 0.9$ K. The value of γ estimated from the analysis of the specific heat is large, $\sim 520 \text{ mJ/mol}\cdot\text{K}^2$ ($m^* \sim 98 m_e$), indicating that $\text{NdOs}_4\text{Sb}_{12}$ is a possible heavy fermion compound. A cubic CEF analysis suggests two best-fit energy level schemes: (I) Γ_6 (0 K), $\Gamma_8^{(1)}$ (180 K), $\Gamma_8^{(2)}$ (420 K); (II) $\Gamma_8^{(2)}$ (0 K), $\Gamma_8^{(1)}$ (220 K), Γ_6 (600 K), both with a molecular field parameter $\Lambda = 1.39 \text{ Nd}\cdot\text{mol}/\text{cm}^3$. The electrical resistivity data indicate that both s-f exchange and aspherical Coulomb scattering are present in $\text{NdOs}_4\text{Sb}_{12}$.

Low-temperature electrical resistivity data suggest the possible existence of spin-wave excitations below Θ_C . The uncertainty in the CEF-energy-level scheme ground state and the possible existence of spin-wave excitations may be resolved by further neutron scattering experiments.

Acknowledgments

We thank Dr. C. Capan for technical support at NHMFL at Los Alamos and Prof. D. P. Arovas at UCSD for helpful discussions. We also thank S. K. Kim and A. P. Thrall for assistance in sample preparation. Research at UCSD was supported by the U. S. Department of Energy under Grant No. DE-FG02-04ER46105, the U. S. National Science Foundation under Grant No. DMR-0335173, and the National Nuclear Security Administration under the Stewardship Science Academic Alliances program through DOE Research Grant No. DE-FG52-03NA00068. The work at the NHMFL Pulsed Field Facility (Los Alamos National Laboratory) was performed under the auspices of the NSF, the State of Florida and the US Department of Energy.

¹ W. Jeitschko and D. Braun, *Acta Cryst. B* **33**, 3401 (1977).

² N. Takeda and M. Ishikawa, *J. Phys. Soc. Jpn.* **69**, 868 (2000).

³ K. Abe, H. Sato, T. D. Matsuda, T. Nanmiki, H. Sugawara, and Y. Aoki, *J. Phys.: Condens. Matter* **14**, 11757 (2002).

⁴ Y. Aoki, T. Namiki, T. D. Matsuda, K. Abe, H. Sugawara, and H. Sato, *Phys. Rev. B* **65**, 064446 (2002).

⁵ M. B. Maple, E. D. Bauer, V. S. Zapf, E. J. Freeman, N. A. Frederick, and R. P. Dickey, *Acta Phys. Pol. B* **32**, 3291 (2001).

⁶ E. D. Bauer, N. A. Frederick, P.-C. Ho, V. S. Zapf, and M. B. Maple, *Phys. Rev. B* **65**, 100506R (2002).

⁷ E. Bauer, St. Berger, Ch. Paul, M. Della Mea, G. Hilscher, H. Michor, M. Reissner, W. Steiner, A. Grytsiv, P. Rogl, and E. W. Scheidt, *Phys. Rev. B* **66**, 214421 (2002).

⁸ C. Sekine, T. Uchiumi, I. Shirotani, and T. Yagi, *Phys. Rev. Lett.* **79**, 3218 (1997).

⁹ G. P. Meissner, M. S. Torikachvili, K. N. Yang, M. B. Maple, and R. P. Guertin, *J. Appl. Phys.* **57**, 3073 (1985).

¹⁰ M. B. Maple, N. R. Dilley, D. A. Gajewski, E. D. Bauer, E. J. Freeman, R. Chau, D. Mandrus, and B. C. Sales, *Physica B* **259-261**, 8 (1999).

¹¹ A. Leithe-Jasper, D. Kaczorowski, P. Rogl, J. Bogner, M. Reissner, W. Steiner, G. Wiesinger, and C. Godart, *Solid State Commun.* **109**, 395 (1999).

¹² N. Takeda and M. Ishikawa, *Physica B* **259-261**, 92 (1999).

¹³ E. D. Bauer, A. Ślebarski, R. P. Dickey, E. J. Freeman, C. Sirvent, V. S. Zapf, N. R. Dilley, and M. B. Maple, *J. Phys.: Condens. Matter* **13**, 5183 (2001).

¹⁴ E. Bauer, St. Berger, A. Galatanu, Ch. Paul, M. Della Mea, H. Michor, G. Hilscher, A. Grytsiv, P. Rogl, D. Kaczorowski, L. Keller, T. Hermannsdörfer, and P. Fischer, *Physica B* **312-313**, 840 (2002).

¹⁵ M. S. Torikachvili, J. W. Chen, Y. Dalichaouch, R. P. Guertin, M. W. McElfresh, C. Rossel, M. B. Maple, and G. P. Meissner, *Phys. Rev. B* **36**, 8660 (1987).

¹⁶ H. Sato, H. Sugawara, T. Namiki, S. R. Saha, S. Osaki, T. D. Matsuda, Y. Aoki, Y. Inada, H. Shishido, R. Settai, and Y. Onuki, *J. Phys.: Condens. Matter* **15**, S2063 (2003).

¹⁷ N. A. Frederick, T. D. Do, P.-C. Ho, N. P. Butch, V. S. Zapf, and M. B. Maple, *Phys. Rev. B* **69**, 024523 (2004).

¹⁸ T. Cichorek, A. C. Mota, F. Steglich, N. A. Frederick, W. M. Yuhasz, and M. B. Maple, *Phys. Rev. Lett.* **94**, 107002 (2005).

¹⁹ E. E. M. Chia, M. B. Salamon, H. Sugawara, and H. Sato, *Phys. Rev. Lett.* **91**, 247003 (2003).

²⁰ E. E. M. Chia, M. B. Salamon, H. Sugawara, and H. Sato, *Phys. Rev. B* **69**, 180509 (2004).

²¹ C. B. H. Evers, W. Jeitschko, L. Boonk, D. J. Braun, T. Ebel, and U. D. Scholz, *J. Alloys Comps.* **224**, 184 (1995).

²² G. M. Sheldrick, SHELXS-97, Program for Crystal Structure Refinements, University of Goettingen, Germany (1997); windows version by McArdle, Natl. Univ. Galway, Ireland.

²³ E. D. Bauer, R. P. Dickey, V. S. Zapf, and M. B. Maple, *J. Phys.: Condens. Matter* **13**, L759 (2001).

²⁴ E. D. Bauer, A. Ślebarski, N. A. Frederick, W. M. Yuhasz, M. B. Maple, D. Cao, F. Bridges, G. Giester, and P. Rogl, *J. Phys.: Condens. Matter* **16**, 5095 (2004).

²⁵ B. C. Sales, B. C. Chakoumakos, D. Mandrus, J. W. Sharp, N. R. Dilley, and M. B. Maple, *Mat. Res. Soc. Symp. Proc.*

²⁶ 545, 13 (1999).

²⁶ R. P. Hermann, R. Jin, W. Schweika, F. Grandjean, D. Mandrus, B. C. Sales, and G. J. Long, *Phys. Rev. Lett.* **90**, 135505 (2003).

²⁷ K. Takegahara, H. Harima, and A. Yanase, *J. Phys. Soc. Jpn.* **70**, 1190 (2001).

²⁸ K. R. Lea, M. J. M. Leask, and W. P. Wolf, *J. Phys. Chem. Solids* **23**, 1381 (1962).

²⁹ P. Fulde, *Handbook on the Physics and Chemistry of rare earths* **2**, 304 (1979).

³⁰ N. H. Andersen, *Crystalline electric field and structural effects in f-electron systems* 373 (1980).

³¹ A. Ślebarski and D. Wohleben, *Z. Phys. B* **60**, 449 (1985).

³² M. B. Maple, Ph. D. thesis, University of California, San Diego (1969).

³³ W. Y. Yuhasz, N. A. Frederick, P.-C. Ho, N. P. Butch, B. J. Taylor, T. A. Sayles, M. B. Maple, J. B. Betts, A. H. Lacerda, P. Rogl, and G. Giester, *Phys. Rev. B* **71**, 104402 (2005).

³⁴ R. Elliott, *Phys. Rev.* **94**, 564 (1954).

³⁵ P. Fulde and I. Peschel, *Advances in Physics* **21**, 1 (1972).

³⁶ N. A. Frederick and M. B. Maple, *J. Phys.: Condens. Matter* **15**, 4789 (2003).

³⁷ K. D. Schotte and U. Schotte, *Phys. Lett.* **55A**, 38 (1975).

³⁸ E. V. Sampathkumaran and I. Das, *Phys. Rev. B* **51**, 8178 (1995).

³⁹ M. Bouvier, P. Lethuillier, and D. Schmitt, *Phys. Rev. B* **34**, 13137 (1991).

⁴⁰ R. Mallik, E. V. Sampathkumaran, J. Dumschat, and G. Wortmann, *Solid State Comm.* **102**, 59 (1997).

⁴¹ M. B. Maple, P.-C. Ho, N. A. Frederick, V. S. Zapf, W. M. Yuhasz, E. D. Bauer, A. D. Christianson, and A. H. Lacerda, *J. Phys.: Condens. Matter* **15**, S2071 (2003).

⁴² H. Sugawara, Y. Abe, Y. Aoki, H. Sato, M. Hedo, R. Settai, Y. Onuki, and H. Harima, *J. Phys. Soc. Jpn.* **69**, 2938 (2000).

⁴³ T. Goto, Y. Nemoto, K. Sakai, T. Yamaguchi, M. Akatsu, T. Yanagisawa, H. Hazama, K. Onuki, H. Sugawara, and H. Sato, *Phys. Rev. B* **69**, 180511(R) (2004).

⁴⁴ A. R. Mackintosh, *Phys. Lett.* **4**, 140 (1963).